Simulation of the Internal Flow Field of Jet Pumps Using the RANS Method

Akbar Ravan Ghalati[1], Manuel Orlando Sandoval Pinto[2], Sergio Croquer Perez[3], Sébastien Poncet[3], Jay Lacey[1], Hakim Nesreddine[4]

[1]Civil Engineering Department, University of Sherbrooke
Sherbrooke J1K2R1, Canada
Akbar.Ravan.Ghalati@usherbrooke.ca; Jay.Lacey@usherbrooke.ca
[2]Department of mechanical and aerospace engineering, Universidad de Antioquia
Medellin, Colombia
manuel.sandoval@udea.edu.co
[3]Mechanical Engineering Department, University of Sherbrooke
Sherbrooke J1K2R1, Canada
sergio.croquer.perez@usherbrooke.ca; Sebastien.Poncet@usherbrooke.ca
[4]Laboratoire des technologies de l'énergie, Hydro-Québec, Shawinigan, Canada
nesreddine.hakim@hydroquebec.com

Abstract - This paper focuses on CFD simulations of the internal flow field of jet pumps, which are passive pumping devices. A numerical method based on the RANS equations is proposed, and its abilities are analysed by comparing the obtained results with the available experimental data. The turbulent flow is simulated using Boussinesq hypothesis which relates Reynolds stresses to the mean velocity gradients via turbulent viscosity. The k-ε model (along with the Standard wall function) and the k-ω SST model are used to calculate the turbulent viscosity for solving the flow in near-wall regions. Before checking the validity of the numerical results, Grid Convergence Index (GCI) is estimated to evaluate the mesh. The analysis showed that the maximum GCI is at the cell near the wall with the value of 0.08%. Comparison of the numerical results and experimental data shows that the model captures the jet pump efficiency range with average relative errors of 7.3% and 8.47% for the k-ε and k-ω SST turbulence models, respectively. The numerical results also confirmed that increasing the flow ratio causes the mixing location between the primary and secondary flows to move toward the outlet of the jet pump, which was observed in the previous experimental investigations. The static pressure coefficient, which indicates the pumping effect of the jet pump, is calculated via both of the turbulence models and the comparison with the experimental data showed that the average relative error is 10.68% and 3.21% for the k-ε model and the k-ω SST model, respectively. The study shows that accurate modelling of jet pump parameters is feasible using RANS approach.

***Keywords*:** Jet pump – RANS modelling - GCI analysis – Pumping effect

1. Introduction

Jet pumps are passive pumping devices which can be utilized for pressurizing and/or displacing a fluid, and operate based on the energy of a primary (motive) fluid [1]. Inside the device, part of the energy of the motive fluid is transferred to a secondary (driven) fluid through momentum exchange processes. Typically, a jet pump consists of four main components, namely: nozzle, suction chamber, mixing throat and diffuser. The primary flow is discharged through a nozzle (in the same manner as a jet) into the mixing throat with high kinetic energy. This process causes a pressure drop in the suction chamber, and the secondary flow is forced into the pump. The two flows enter the mixing throat where the momentum transfer takes place. The mixed flow then passes the diffuser where its kinetic energy is converted to pressure energy, and the desired pumping effect is achieved [2].

Jet pumps have been employed in various applications because of their simplicity and high reliability, absence of lubricants or bearings [3] and low installation costs [4]. Xiao et al. [5] used a jet pump as a potential tool for conveying fish in the aquatic industry. These devices can also be employed for transportation of hazardous liquids or rocks with limited dimensions [6]. Several applications of jet pumps as a boosting system are discussed in the study of Peeran et al. [7].

The performance of jet pumps can be investigated using 1D theoretical models, Computational Fluid Dynamics (CFD) models and experimental methods. 1D theoretical modelling refers to using the integral forms of conservation equations for calculating the flow parameters at predefined cross sections of the jet pump. Winoto et al. [8] used this approach to study the performance of a jet pump with water for both the primary and the secondary flow. The governing equations of the 1D model contained the friction loss coefficient for each component of the jet pump. The friction loss coefficient of the primary nozzle was obtained experimentally, and the value for the suction chamber, mixing throat and diffuser were defined based in previous literature which makes the model case dependent. Cunningham [9] proposed a 1D theoretical model for liquid-gas jet pumps. The introduced 1D model represented the flow behaviour as long as the mixing shock is located in the mixing throat. Cunningham and Dopkin [10] experimentally observed that the assumption of constant friction coefficients for modelling liquid jet pumps is satisfactory if complete mixing occurs inside the throat. Otherwise, the coefficients are highly dependent on the flow rate of the jet pump. It can be concluded that the 1D theoretical approach is an efficient method in terms of computational costs. However, their functionality is very limited since it requires the empirical adjustment of the friction loss coefficients for closing the system equations.

CFD models are an alternative method for studying jet pumps. This method allows the exploration of effects of geometrical [11], [12] and operational parameters [13], [14] on jet pump performance and the internal flow field [15]. Xu et al. [16] used Large Eddy Simulation (LES) to investigate the turbulent flow field of an annular jet pump. The numerical domain contained more than 11×10^6 cells. Although great details of the flow were represented by LES, the large computational cost of the method restricts its application. The Reynolds-averaged Navier–Stokes (RANS) approach is a less computationally expensive technique which can be used for modelling the turbulent flow field of single-phase [17] and multi-phase jet pumps [18]. This approach not only features acceptable accuracy [15], but also requires fewer computational sources than other approaches such as Direct Numerical Simulation (DNS) and LES [19]. In this regard, the present study aims to introduce a validated CFD tool based on the RANS for simulating jet pumps.

The paper is organized in the following manner: Section 2 describes the numerical method. Details about the numerical domain and the results of the grid sensitivity analysis are provided in Section 3. The validation is shown in Section 4, followed by the most relevant conclusions in Section 5.

2. Numerical Methods

The RANS approach (in the steady and incompressible form) is used here for the simulation of the flow field in liquid jet pumps. In this approach, the field variables (velocity components, pressure and other quantities) of the instantaneous Navier-Stokes equations are decomposed into the mean and fluctuating components [20]. The procedure results in additional averaged products (Reynolds stresses) which represent turbulent fluctuations of momentum and must be modelled. One of the approaches for modelling turbulent flows is using Boussinesq hypothesis which relates Reynolds stresses to the mean velocity gradients [21] through the turbulent viscosity (μ_t). Two closures are compared here, namely, the Realizable k-ε model [22] (along with the standard wall function [23]) and the k-ω SST model [24]. In the realizable k-ε model, two transport equations for the turbulence kinetic energy, k, and the turbulence dissipation rate, ε, are solved. The k-ω SST model uses the k-ω model [25] in the near wall regions while the k-ε model is used for regions away from the wall. The transport equation of the specific dissipation rate, ω, is also solved.

The flow field is numerically simulated using a pressure-based solver, in which the velocity field is obtained from the momentum equations and the pressure field is calculated by solving a pressure correction equation obtained by manipulating continuity and momentum equations, available in ANSYS Fluent 2022R1. The governing equations for the conservation of mass, momentum and turbulence are solved using a control-volume-based technique that consists of discretization of the integral governing equation on the computational grid and linearization of the discretized equations. The spatial discretization is achieved by a second-order upwind scheme [26], while a second-order method is used for the calculation of pressure at the cell faces [20]. The gradients of all variables are computed based on the least squares cell-based gradient method [20]. The mass flux through the cell faces is calculated using the Rhie and Chow method [27], and the SIMPLE algorithm enables to overcome the pressure-velocity coupling [28]. Finally, the obtained linear system of equations is solved by the Gauss-Seidel method [20].

3. Numerical Domain and Grid Sensitivity Analysis

The numerical domain is designed based on the water jet pump used in the experiments of Sanger [29], which used water for both the primary and secondary flows. The area ratio (ratio of the primary nozzle area to the mixing throat area) of the selected jet pump is 0.197 and there is no space between the primary nozzle outlet and the mixing throat. The mixing throat length and diameter are 194 mm and 34.2 mm, respectively. The diffuser length is 490 mm and its angle is 6°. The objective of the experiments was to analyse the performance of the jet pump over a wide range of operational and geometrical conditions. Fig. 1 shows the adopted 2D axisymmetric numerical domain along with the boundary conditions and the structured grid system. Based on the experiments of Sanger [29] the mass flow rate of the primary flow and the pressure of the secondary flow are fixed to 3.97 kg/s and 103 kPa, respectively. The mass flow rate of the outlet is changed to reach various flow ratios ($M = \frac{Q_2}{Q_1}$, where Q_2 and Q_1 are volume flow rates of the secondary and primary flows). A turbulence intensity (the ratio of the root-mean-square of the velocity fluctuations to the mean flow velocity) of 5% and a turbulent viscosity ratio (μ_t/μ) of 10 are imposed at both flow inlets for specification of the turbulence quantities. No-slip condition is imposed to all walls.
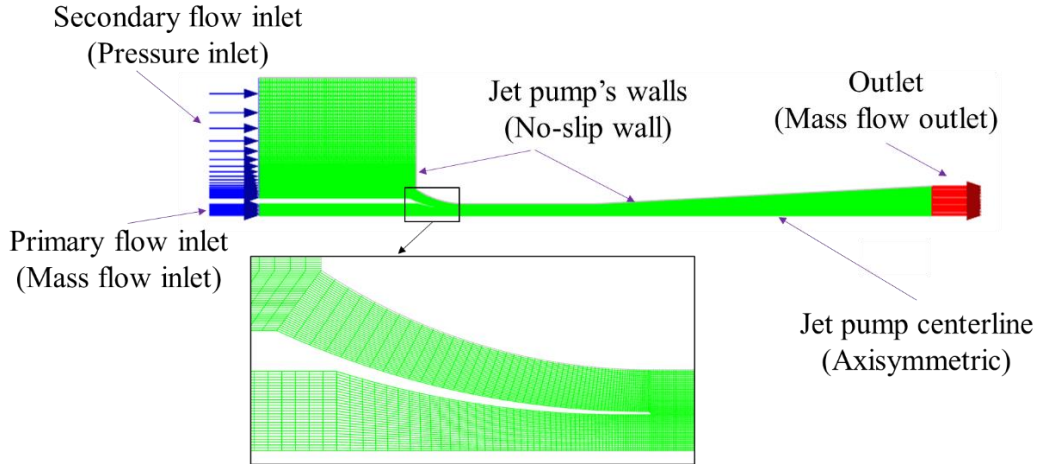

Fig. 1: The boundary locations and conditions of the simulated of the jet pump and the 33k structured grid system.

In this study, the Grid Convergence Index (GCI) is adopted to estimate the discretization error of the k-ε simulations based on Richardson extrapolation. As it is recommended in [30], three different grids are generated for GCI analysis. The coarse, medium and fine grids contain 16749 ($\approx$16k mesh), 33220 ($\approx$33k mesh) and 54226 ($\approx$54k mesh) structured cells, respectively. Fig. 1 shows the 16k mesh as an example. The numerical data achieved from the total pressure ($p + \rho v^2/2$) profile at x/d$_t$ = 4.8 (where x-axis origin is located at the outlet of the primary nozzle and d$_t$ is the mixing throat diameter) when M=1.6 is used for GCI analysis. The representative grid size for a 2D grid system is calculated using $h = \left[\frac{1}{N}\sum_{i=1}^{N} A_i\right]^{0.5}$, where A_i is the area of the i_{th} cell, and N is the total number of cells used for the computations. The representative cell size for 16k, 33k and 54k mesh systems at x/d$_t$ = 4.8 are 7.5$\times$ 10^{-4} m, 5.48$\times$ 10^{-4} m and 3.7$\times$ 10^{-4} m, respectively. If h$_1$<h$_2$<h$_3$ and r$_{21}$=h$_2$/h$_1$ and r$_{32}$=h$_3$/h$_2$, the apparent order of accuracy, p, is calculated using Eqs. (1) and (2):

$$p = \frac{1}{\ln(r_{21})}|\ln|\varepsilon_{32}/\varepsilon_{21}| + q(p)| \tag{1}$$

$$q(p) = \ln\left(\frac{r_{21}{}^p - s}{r_{32}{}^p - s}\right) \tag{2}$$

where $s = 1 \times sign(\varepsilon_{32}/\varepsilon_{21})$, ε_{32}=φ_3- φ_2, ε_{21}=φ_2- φ_1 and φ_k denotes the solution of φ on the kth grid system. $e_a^{21} = |(\phi_1 - \phi_2)/\phi_1|$ is the approximate relative error and the grid convergence index is calculated using

$GCI_{fine}^{21} = 1.25e_a^{21}/(r_{21}{}^p - 1)$). The analysis showed that the maximum GCI is at the cell near the wall with the value of 0.08%. It should be mentioned that 88% of the points showed the oscillatory convergence (ε_{32} / ε_{21}<0). The local order of accuracy (p) calculated using Eq. 1 is in the range of 0.6 to 10.7, with the average value of 5.2 which shows the high accuracy of the simulations. Additionally, the maximum approximate relative error is 1.2% for the mentioned cross section. Fig. 2 shows the comparison between the numerical total pressure calculated via the various grid systems at x/d$_t$ = 4.8.

It can be concluded from the GCI analysis that the numerical results obtained using k-ε turbulence model are grid-convergent. Consequently, the 33k grid system is selected for the next simulations.
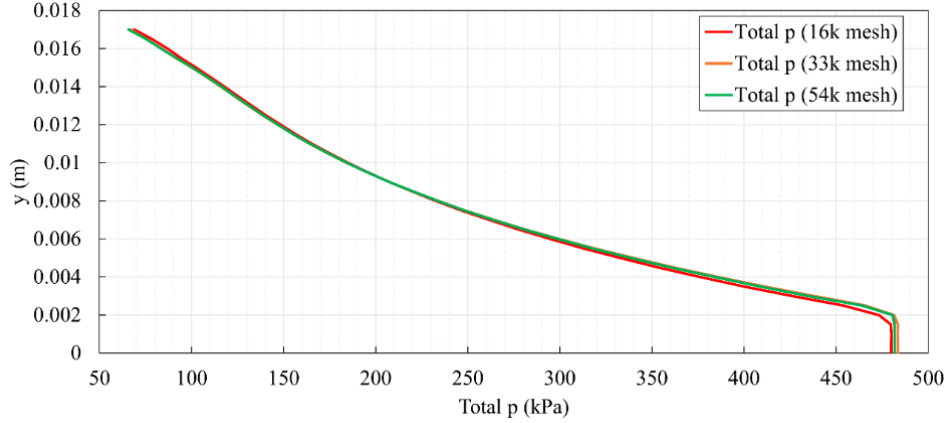

Fig. 2: The numerical total pressure calculated via three different grid systems at x/d$_t$ = 4.8 when M=1.6.

It has to be noted that since no wall function is used for the simulation with the k-ω SST turbulence model, the mesh system is refined for resolving the flow field in the near wall regions. Both structured (with the same pattern shown in Fig. 1) and unstructured (triangular) girds are generated for the simulation with the k-ω SST turbulence model. To ensure that the adequate number of grids has been generated for resolving the boundary layer, the velocity profile at x/d$_t$=2.84 (middle of the mixing throat) is compared against the Standard law of wall curves in Fig. 3. y^+ in this figure is the non-dimensional distance from the wall and calculated via yu_τ/ν, where y is the vertical distance from the wall, u_τ is the friction velocity ($= \sqrt{\frac{\tau_w}{\rho}}$ where τ_w is the wall shear stress and ρ is density), and ν is the kinematic viscosity. The vertical axis shows u^+ which is the dimensionless streamwise velocity (u/u_τ). The agreement between the numerical results and the universal boundary layer velocity profile confirms that the utilized grid is fine enough for capturing the flow field in the near wall regions.

4. Validation

In this section, the results obtained from the introduced numerical model will be compared with the experimental data reported in Sanger [29]. One of the main parameters that can be used for evaluating the performance of the jet pumps is efficiency (η), which is calculated as [8]:

$$\eta = \frac{Q_2}{Q_1} \times \frac{P_{out} - P_{sec.}}{P_{prim.} - P_{out}} \tag{3}$$

where Q_2 and Q_1 are volume flow rates of the secondary and primary flows, respectively. P_{out}, $P_{prim.}$ and $P_{sec.}$ are, respectively, the total pressure at the outlet, the primary flow inlet and the secondary flow inlet. It must be noted that various flow ratios were achieved in the experiments by manipulating P_{out} using a valve located downstream of the jet pump outlet.
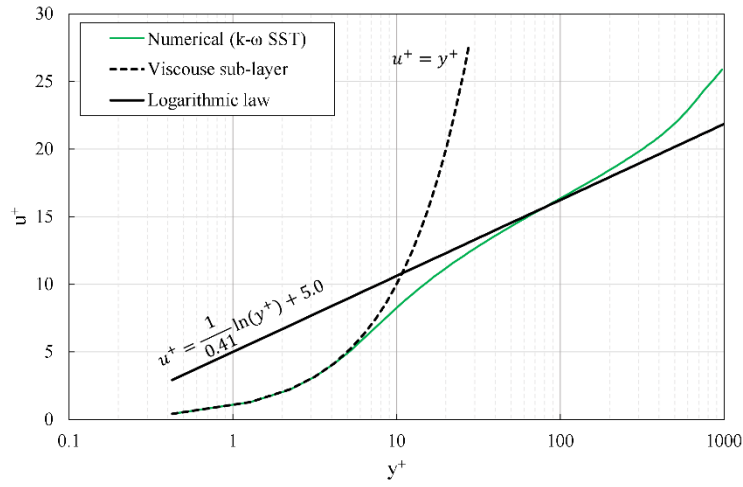
Fig. 3: Comparison of the numerical boundary layer velocity profile with standard law of wall at x/d$_t$=2.84 when M=1.6.

Fig. 4 shows the comparison between numerical and experimental efficiency of the jet pump at various flow ratios ($M = \frac{Q_2}{Q_1}$). The figure shows that the numerical model captured the efficiency variation reasonably well. Additionally, it correctly captures the maximum efficiency position at M=1.4. The average relative errors of the k-ε and k-ω SST simulations are 7.3% and 8.47%, respectively.
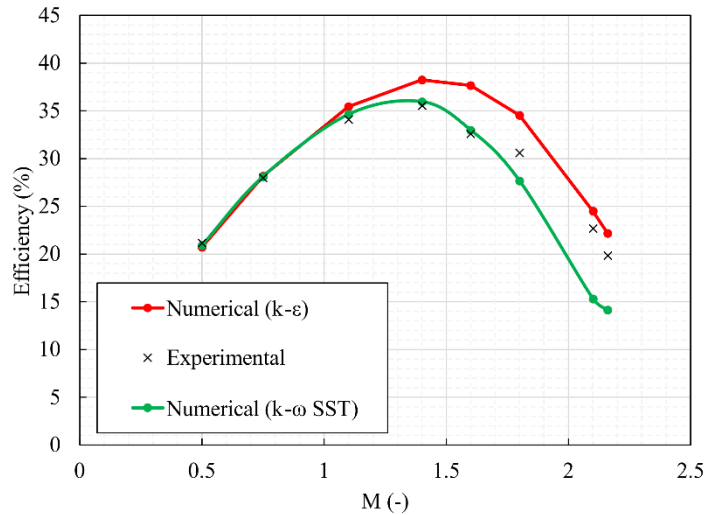

Fig. 4: Efficiency of the jet pump against the flow ratio, $M = \frac{Q_2}{Q_1}$. Comparisons between the numerical results and data of Sanger [29].

The velocity magnitude contours (obtained via k-ε simulations) for various flow ratios are depicted in Fig. 5. The figure shows that increasing the flow ratio causes the mixing location between the primary and secondary flows, which can be indicated by the primary jet's core disappearance, to move toward the outlet of the jet pump. It can be seen that when M=1.4, the mixing between the primary and secondary flows is completed near the throat exit. M=1.4 is the flow ratio in which the jet pump operates with the maximum efficiency based on Fig. 4. It can be concluded that if the operation with maximum efficiency is desired, the mixing zone should be located near the throat exit. Fig. 5 also shows that when M=2.16 the primary jet reaches the diffuser which leads to efficiency drop as showed in Fig. 4. This phenomenon is clearly observed in the experiments of Cunningham [9] and the efficiency drop was attributed to the sudden expansion losses.

The numerical results and experimental pressure coefficient distributions along the jet pump's wall for M=1.6 are shown in Fig. 6. The pressure coefficient is calculated via $C_p = \frac{p - p_{sec.}}{\rho v^2 / 2}$, where p is the static pressure along the jet pump's wall and v is velocity of the primary flow at the primary nozzle outlet.
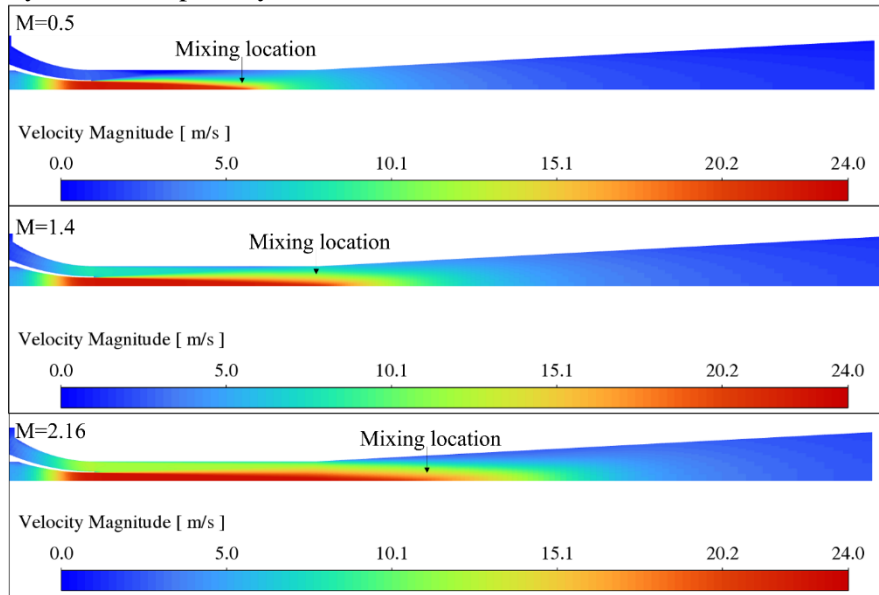

Fig. 5: Contours of the velocity magnitude achieved using the k-ε model for various flow ratios.

The simulations with the both turbulence models successfully reflect the static pressure rise (pumping effect) in the diffuser. The average relative error between k-ε simulation and experimental data is 10.68%, while the disagreement of the k-ω SST simulation with the experimental data is 3.21%.

Fig. 7 depicts the comparison of the calculated total pressure profile via the k-ε and the k-ω SST turbulence models (normalized by the maximum value of the total pressure) with the experimental results at three different cross sections. The profile shows that part of the jet is still not mixed with the secondary flow at cross sections x/d_t=2.6 and x/d_t=4.8 (considering that the length of the mixing throat is 5.66d_t). The numerical results obtained via both of the utilized turbulence models reasonably agree with the experimental data, and the variation trend is captured by the numerical models.

5. Conclusions

A 2D RANS solver using various turbulence models is introduced. The following conclusions can be drawn:

- GCI analysis showed that the numerical solution achieved by the k-ε turbulence model is grid independent with a maximum GCI of 0.08%. Comparison of the velocity profile obtained by the k-ω SST turbulence model with the universal boundary layer profile confirmed that the model reflects the flow field near in the near-wall regions.

- The simulation of the jet pump in various operating conditions using the k-ε and k-ω SST turbulence models showed that both models are able to capture the efficiency behaviour of the device with an average disagreement of 7.3% and 8.47% relative to experimental data. Similarly, the average deviation from the experimental data in terms of the pressure coefficient along the mixing throat and diffuser is 10.68% for the k-ε turbulence model, while the error for the k-ω SST simulation is reduced to 3.21%.

- The numerical velocity magnitude contours show that by increasing the flow ratio of the device, the mixing zone between the primary and secondary flow moves toward the outlet of the jet pump.

- The comparison of the numerical and experimental total pressure profile showed that the introduced model successfully reflects the internal flow field.
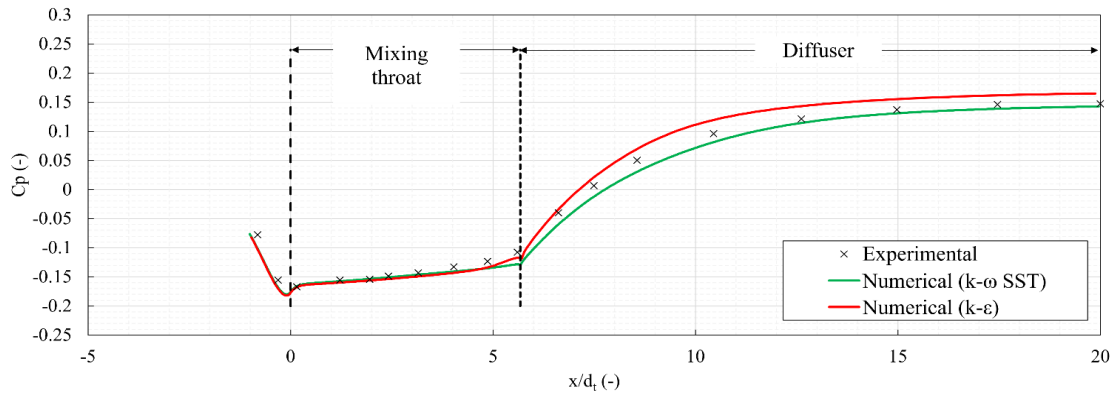
Fig. 6: Static pressure coefficient (C_p) against non-denationalized horizontal location (x/d_t) when M=1.6. Comparisons between the numerical results and the experimental data of Sanger [29].
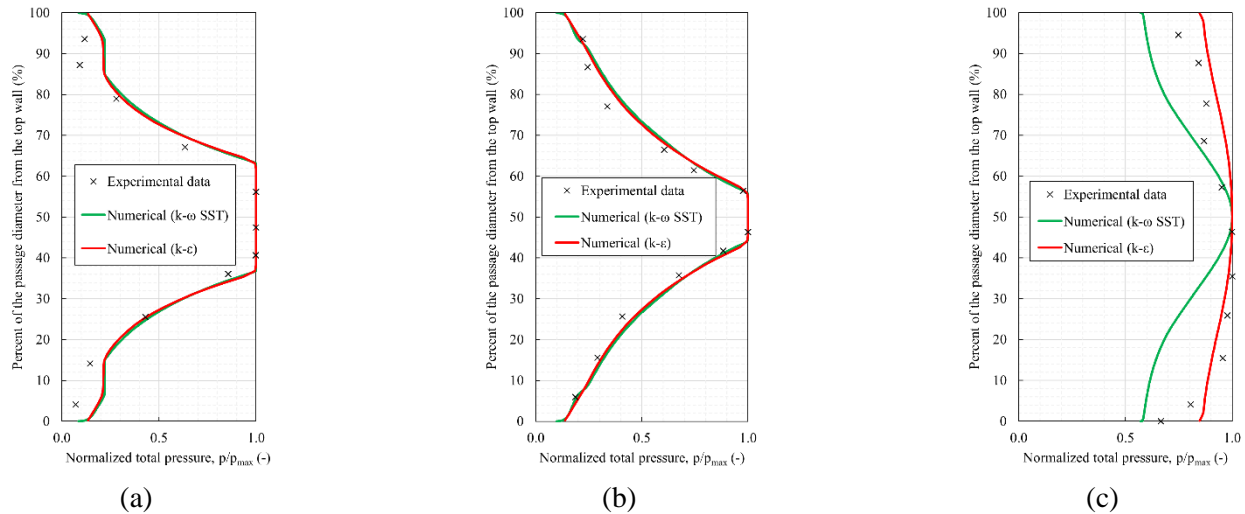

| (a) | (b) | (c) |

Fig. 7: Total pressure profile at (a) x/d_t=2.6, (b) x/d_t=4.8 and (c) x/d_t=10.4 when M=1.6. Comparisons between the numerical results and the experimental data of Sanger [29].

Acknowledgements

References

[1] I. J. Karassik, J. P. Messina, P. Cooper, and C. C. Heald, *Pump handbook*, vol. 3. McGraw-Hill New York, 2001.

[2] T. Tan, J. Liu, H. Chen, and W. Lu, "Review and Comparison of Ejectors Design Methods and Their Application," in *ASME International Mechanical Engineering Congress and Exposition*, Montreal, vol. 46552, V08AT10A087, 2014.

[3] A. B. Little, S. Garimella, and J. P. DiPrete, "Combined effects of fluid selection and flow condensation on ejector operation in an ejector-based chiller," *Int. J. Refrig.*, vol. 69, pp. 1–16, 2016.

[4] K. O. Shestopalov, B. J. Huang, V. O. Petrenko, and O. S. Volovyk, "Investigation of an experimental ejector refrigeration machine operating with refrigerant R245fa at design and off-design working conditions. Part 2. Theoretical and experimental results," *Int. J. Refrig.*, vol. 55, pp. 212–223, 2015.

[5] L. Xiao, X. Long, L. Li, M. Xu, N. Wu, and Q. Wang, "Movement characteristics of fish in a jet fish pump," *Ocean Eng.*, vol. 108, pp. 480–492, 2015.

[6] E. Lisowski and H. Momeni, "CFD modeling of a jet pump with circumferential nozzles for large flow rates," *Arch. Foundry Eng.*, vol. 10, no. 3, pp. 69–72, 2010.

[7] S. M. Peeran, N. Beg, and S. Sarshar, "Novel examples of the use of surface jet pumps (SJPs) to enhance production & processing. Case studies & lessons learnt," in *SPE North Africa Technical Conference and Exhibition*, Cairo, SPE-165382, 2013.

[8] S. H. Winoto, H. Li, and D. A. Shah, "Efficiency of Jet Pumps," *J. Hydraul. Eng.*, vol. 126, no. 2, pp. 150–156, 2000.

[9] R. G. Cunningham, "Gas compression with the liquid jet pump," *J. Fluids Eng.*, vol. 96, no. 3, pp. 203-215, 1974.

[10] R. G. Cunningham and R. J. Dopkin, "Jet breakup and mixing throat lengths for the liquid jet gas pump," *J. Fluids Eng.*, vol. 96, no. 3, pp. 216-226, 1974.

[11] M. T. Kandakure, V. G. Gaikar, and A. W. Patwardhan, "Hydrodynamic aspects of ejectors," *Chem. Eng. Sci.*, vol. 60, no. 22, pp. 6391–6402, 2005.

[12] K. Aldaş and R. Yapıcı, "Investigation of Effects of Scale and Surface Roughness on Efficiency of Water Jet Pumps Using CFD," *Eng. Appl. Comput. Fluid Mech.*, vol. 8, no. 1, pp. 14–25, 2014.

[13] J. Zhao, X. Wei, J. Zou, Y. Zhang, J. Sun, and Z. Liu, "Research on performance optimization of gas–liquid ejector in multiphase mixed transportation device," *J. Mech.*, vol. 38, pp. 22–31, 2022.

[14] H. Li, H. Li, X. Huang, Q. Han, Y. Yuan, and B. Qi, "Numerical and experimental study on the internal flow of the venturi injector," *Processes*, vol. 8, no. 1, article 64, 2020.

[15] X. Wang, H. Li, J. Dong, J. Wu, and J. Tu, "Numerical study on mixing flow behavior in gas-liquid ejector," *Exp. Comput. Multiph. Flow*, vol. 3, no. 2, pp. 108–112, 2021.

[16] M. Xu, X. Yang, X. Long, and Q. Lü, "Large eddy simulation of turbulent flow structure and characteristics in an annular jet pump," *J. Hydrodyn.*, vol. 29, no. 4, pp. 702–715, 2017.

[17] X. L. Yang and X. P. Long, "Numerical investigation on the jet pump performance based on different turbulence models," in *IOP Conference Series: Earth and Environmental Science*, vol. 15, no. 5, article 052019, 2012.

[18] L. Asfora, A. dos Santos, and L. de Jesus Nogueira Duarte, "Modeling multiphase jet pumps for gas compression," *J. Pet. Sci. Eng.*, vol. 173, pp. 844–852, 2019.

[19] Y. A. Çengel and J. M. Cimbala, "Fluid Mechanics: Fundamentals and Applications, Fourth Edition." New York: McGraw-Hill Education, 2018.

[20] Ansys® Fluent, 2022R1, help system, Fluent Theory Guide ,ANSYS, Inc.

[21] S. B. Pope, *Turbulent flows*. Cambridge university press, 2000.

[22] T. H. Shih, W. W. Liou, A. Shabbir, Z. Yang, and J. Zhu, "A new k-ϵ eddy viscosity model for high reynolds number turbulent flows," *Computers & Fluids*, vol. 24, no. 3, pp. 227–238, 1995.

[23] B. E. Launder and D. B. Spalding, "The numerical computation of turbulent flows," in *Numerical prediction of flow, heat transfer, turbulence and combustion*, Elsevier, pp. 96–116, 1983.

[24] F. R. Menter, "Two-equation eddy-viscosity turbulence models for engineering applications," *AIAA J.*, vol. 32, no. 8, pp. 1598–1605, 1994.

[25] D. C. Wilcox, "Reassessment of the scale-determining equation for advanced turbulence models," *AIAA J.*, vol. 26, no. 11, pp. 1299–1310, 1988.

[26] T. Barth and D. Jespersen, "The design and application of upwind schemes on unstructured meshes," in *27th Aerospace Sciences Meeting*, Reno, 1989.

[27] C. M. Rhie and W. L. Chow, "Numerical study of the turbulent flow past an airfoil with trailing edge separation," *AIAA J.*, vol. 21, no. 11, pp. 1525–1532, 1983.

[28] S. V. Patankar and D. B. Spalding, "A calculation procedure for heat, mass and momentum transfer in three-dimensional parabolic flows," *Int. J. Heat Mass Transf.*, vol. 15, no. 10, pp. 1787–1806, 1972.

[29] N. L. Sanger, "Noncavitating and cavitating performance of two low-area-ratio water jet pumps with throat lengths of 5.66 diameters," National Aeronautics and Space Administration, 1968.

[30] I.B. Celik, U. Ghia, P.J. Roache, C.J. Freitas, H. Coleman and P.E. Raad, "Procedure for Estimation and Reporting of Uncertainty Due to Discretization in CFD Applications," *J. Fluids Eng.*, vol. 130 (7), no. 078001, 2008.